Published in final edited form as:
Pain. 2014 November ; 155(11): 2377–2389. doi:10.1016/j.pain.2014.09.007.

Autoimmunity contributes to nociceptive sensitization in a mouse model of complex regional pain syndrome

Wen-Wu Li[a,b,c], **Tian-Zhi Guo**[a], **Xiaoyou Shi**[a,b,c], **Eva Czirr**[d,e], **Trisha Stan**[d,e], **Peyman Sahbaie**[b,c], **Tony Wyss-Coray**[d,e], **Wade S. Kingery**[a], and **J. David Clark**[b,c,*]

[a]Physical Medicine and Rehabilitation Service, Veterans Affairs Palo Alto Health Care System, Palo Alto, CA, USA

[b]Anesthesiology Service, Veterans Affairs Palo Alto Health Care System, Palo Alto, CA, USA

[c]Department of Anesthesia, Stanford University School of Medicine, Stanford, CA, USA

[d]Center for Tissue Regeneration, Repair, and Restoration, Veterans Affairs Palo Alto Health Care System, Palo Alto, CA, USA

[e]Department of Neurology and Neurological Sciences, Stanford University School of Medicine, Stanford, CA, USA

Abstract

Complex regional pain syndrome (CRPS) is a painful, disabling, chronic condition whose etiology remains poorly understood. The recent suggestion that immunological mechanisms may underlie CRPS provides an entirely novel framework in which to study the condition and consider new approaches to treatment. Using a murine fracture/cast model of CRPS, we studied the effects of B-cell depletion using anti-CD20 antibodies or by performing experiments in genetically B-cell-deficient (μMT) mice. We observed that mice treated with anti-CD20 developed attenuated vascular and nociceptive CRPS-like changes after tibial fracture and 3 weeks of cast immobilization. In mice with established CRPS-like changes, the depletion of CD-20+ cells slowly reversed nociceptive sensitization. Correspondingly, μMT mice, deficient in producing immunoglobulin M (IgM), failed to fully develop CRPS-like changes after fracture and casting. Depletion of CD20+ cells had no detectable effects on nociceptive sensitization in a model of postoperative incisional pain, however. Immunohistochemical experiments showed that CD20+ cells accumulate near the healing fracture but few such cells collect in skin or sciatic nerves. On the other hand, IgM-containing immune complexes were deposited in skin and sciatic nerve after fracture in wild-type, but not in μMT fracture/cast, mice. Additional experiments demonstrated that complement system activation and deposition of membrane attack complexes were partially blocked by anti-CD20+ treatment. Collectively, our results suggest that CD20-positive B cells produce antibodies that ultimately support the CRPS-like changes in the murine fracture/cast model. Therapies directed at reducing B-cell activity may be of use in treating patients with CRPS.

*Corresponding author at: Anesthesia Service, Veterans Affairs Palo Alto Health Care System, 3801 Miranda Ave., Palo Alto, CA 94304, USA. Tel.: + 1 650 493 5000x67184; fax: + 1 650 852 3423. djclark@stanford.edu (J.D. Clark).

Conflict of interest statement

The authors do not have financial or other relationships that might lead to conflict of interest.

Keywords

Autoimmunity; B cell; Complex regional pain syndrome; Pain; Fracture

1. Introduction

Complex regional pain syndrome (CRPS) is a painful, disabling, and often chronic condition. Acute CRPS often improves over the first year, particularly if therapy is initiated early in the course of the condition [1]. However, CRPS present for a period of 1 year or greater seldom spontaneously resolves [55], and worsens in most patients from years 1 to 8 after onset [65]. More than 80% of patients with chronic CRPS are severely disabled [59]. Current therapies for CRPS include physical, interventional, pharmacological, and alternative approaches [7, 11]. Unfortunately, the effectiveness of most of these therapies is limited, and no therapy reliably cures chronic CRPS. The syndrome encompasses a disparate collection of signs and symptoms involving the sensory, motor, and autonomic nervous systems, bone demineralization, skin growth changes, and vascular dysfunction, all limited to a single extremity in most cases [40]. Our lack of understanding of the pathophysiological mechanisms supporting this enigmatic condition limits our ability to predict susceptibility and prevents the rational design of new therapies. The recent suggestion that CRPS may be supported by immunological mechanisms provides an entirely novel framework in which to study CRPS and consider new approaches to treatment.

Identifying an autoimmune mechanism for CRPS might help to explain the broad nature of the syndrome’s signs and symptoms as well as difficulties in achieving adequate symptom control, remission, or cure using standard therapies. Exploration of CRPS-related immune system activation began with the serendipitous observation of symptom improvement in CRPS patients treated with intravenous immunoglobulin (IVIG) for unrelated conditions [15]. Eventually, a randomized trial of low-dose IVIG showed intermediate duration control of CRPS symptoms in some patients [14]. An autoimmune mechanism was suggested by experiments demonstrating that immunoglobulin G (IgG) prepared from the sera of CRPS patients bound to cultured autonomic neurons, with little evidence of such interactions when sera from patients with other types of neuropathies were used [30]. Later experiments using a beating cardiomyocyte preparation suggested that most CRPS, but not healthy, patients had autoantibodies binding to and activating the M-2 muscarinic and/or the β-2 adrenergic receptor [29]. Additional evidence for autoimmune mechanisms in CRPS includes genetic data supporting CRPS associations with specific human leukocyte antigens [9, 62, 64], studies showing that IgG from CRPS patients worsens nociceptive sensitization in laboratory animals [61], and case reports of Langerhans antigen presenting cell proliferation in CRPS-affected skin [4]. While many of the aforementioned data involve small patient numbers and heterogeneous patient populations, these intriguing reports suggest that autoimmune mechanisms may support CRPS.

Our group has worked extensively with a rodent model of CRPS involving tibial fracture followed by weeks of cast immobilization [18]. It has been used successfully to study the effects of fracture on neuropeptide signaling, the sympathetic nervous system, mast cell

infiltration, epidermal cytokine production, and other CRPS-related phenomena [20, 36, 37, 52].We hypothesized that we would discover evidence of autoimmunity contributing to the nociceptive and neurovascular CRPS-like changes manifest in this model.

2. Materials and methods

2.1. Animals

All animal experiment protocols were approved by the Veterans Affairs Palo Alto Health Care System Institutional Animal Care and Use Committee (Palo Alto, CA, USA) and followed the animal subjects guidelines of the International Association for the Study of Pain. Male C57BL/6J mice and μMT mice in the same background strain were obtained from The Jackson Laboratory (Sacramento, CA, USA) at 8–12 weeks of age. Experiments were done after a 7–10-day acclimation period in our animal care facility. The animals were housed 4 per cage under pathogen-free conditions with soft bedding and were given food and water ad libitum, with a 12:12 light:dark cycle. The animals were fed Teklad lab rodent diet 2018 (Teklad Diets; Harlan Laboratories, Indianapolis, IN, USA), which contains 1.0% calcium, 0.7% phosphorus, and 1.5 IU/g vitamin D3. Data collection was conducted blind to group assignment.

2.2. Surgery

The mouse fracture model was used [20]. Under isoflurane anesthesia, a hemostat was used to make a closed fracture of the right tibia just distal to the middle of the tibia. The hind limb was then wrapped in casting tape (Delta-Lite; BSN Medical, Hamburg, Germany) so the hip, knee, and ankle were all fixed. The cast extended from the metatarsals of the hind paw up to a spica formed around the abdomen. A window was left open over the dorsal paw and ankle to prevent constriction if postfracture edema developed. After fracture and casting, the mice were given, subcutaneously, 2 days of buprenorphine (0.05 mg/kg) and baytril (5 mg/kg), as well as 1.0 mL of normal saline to maintain hydration. At 3 weeks after surgery, the mice were anesthetized with isoflurane and the cast removed. All mice had union at the fracture site, by manual inspection.

The mouse hind paw incision model was used [45]. Mice were anesthetized using isoflurane 3% in an induction chamber and transferred to the operating table receiving isoflurane 2% (2L of oxygen) delivered through a nose cone. After sterile preparation, a 5-mm longitudinal incision was made with a number 11 scalpel on the plantar surface of the right hind paw. This incision was sufficiently deep to divide deep tissues. Next, the plantaris muscle was dissected longitudinally. After controlling bleeding, a single 6-0 nylon suture was placed through the midpoint of the wound and antibiotic ointment was applied. Nociceptive testing took place at time points up to 7 days after incision.

2.3. B-cell depletion/deficiency experiments in the fracture CRPS models

Three sets of experiments were performed to test the hypothesis that B cells can regulate cutaneous inflammation and nociceptive thresholds after fracture. In the first set of experiments, mice underwent a right distal tibia fracture and were casted. After 1 week of cast immobilization, they were treated with anti-mouse CD20 antibody (rituximab) or

control IgG 5D2 clone (200 μg in 100 μL volume) supplied by Genentech (South San Francisco, CA, USA) via intravenous tail vein injection; groups of nonfracture control mice treated with either control IgG or anti-CD20 served as controls. Hind paw nociceptive testing and assessment of warmth and edema were performed at 3 weeks after fracture following cast removal, and in intact control mice. After completion of nociceptive and physiological measurements, blood was obtained by terminal cardiac puncture and processed for flow cytometry to evaluate the efficiency of B-cell depletion as described below.

Second, we used B-cell-deficient mice (μMT) and C57BL/6J wild-type controls (Jackson Laboratory). Fracture/casting and testing procedures were as described for B-cell depletion experiments.

Lastly, we tested the efficacy of B-cell depletion therapy by antiCD20 in the CRPS model after nociceptive and vascular changes were established. Mice underwent tibia fracture and were casted for 3 weeks. Following cast removal and the completion of initial nociceptive and physiological testing, mice were treated with mouse anti-CD20 or control IgG as described above. Groups of nonfracture mice treated with either control nonimmune IgG or anti-CD20 served as controls. Hind paw nociceptive testing and physiological testing were then performed 1, 7, 14, 21, and 28 days after antibody injection.

2.4. B-cell-depletion experiments in the mouse hind paw incisional model

To test if B cell contributes to all trauma-related pain syndromes, hind paw incisional model of postsurgical pain was employed. Mice received anti-CD20 antibody or control IgG 5D2 clone (200 μg/100 μL, Genentech) once via tail vein intravenous injection 24 hours before performing the surgery.

2.5. Hind paw nociceptive testing

To measure mechanical allodynia in the mice, an up-down von Frey testing paradigm was used as previously described [18, 19, 27, 38]. Briefly, mice were placed on wire mesh platforms in clear cylindrical plastic enclosures 10 cm in diameter and 40 cm in height, and after 15 minutes of acclimation, von Frey fibers of sequentially increasing stiffness were applied against the hind paw plantar skin at approximately midsole, taking care to avoid the tori pads, and pressed upward to cause a slight bend in the fiber and left in place for 5 seconds. Withdrawal of or licking the hind paw after fiber application was scored as a response. When no response was obtained, the next stiffest fiber in the series was applied to the same paw; if a response was obtained, a less stiff fiber was applied. Testing proceeded in this manner until 4 fibers had been applied. Estimation of the mechanical withdrawal threshold by data-fitting algorithm permitted the use of parametric statistics for analysis [46]. Hind paw mechanical nociceptive thresholds were analyzed as the difference between the fractured side (right hind paw) and the contralateral unfractured side (left hind paw), or absolute values in the hind paw incision model.

An incapacitance device (IITC Inc. Life Science, Woodland Hills, CA, USA) was used to measure hind paw unweighting. The mice were manually held in a vertical position over the apparatus with the hind paws resting on separate metal scale plates, and the entire weight of

the mouse was supported on the hind paws. The duration of each measurement was 6 seconds, and 6 consecutive measurements were taken at 10-second intervals. All 6 readings were averaged to calculate the bilateral hind paw weight-bearing values [18, 19, 27]. Right hind paw weight-bearing data were analyzed as a ratio between the right hind paw weight and the sum of right and left hind paw values ([2R/(R + L)] × 100%).

2.6. Hind paw volume testing

A laser sensor technique was used to determine the dorsal-ventral thickness of the hind paw, as we have previously described [38]. The measurement sensor device used in these experiments (Limab, Göteborg, Sweden) has a measurement range of 200 mm, with a 0.01-mm resolution. Hind paw volume data were analyzed as the difference between the fractured side and the contralateral unfractured side.

2.7. Hind paw temperature testing

The temperature of the hind paw was measured using a fine-wire thermocouple (Omega Engineering Inc, Stamford, CT, USA) applied to the paw skin, as previously described [38]. The investigator held the wire using an insulating styrofoam block. Three sites were tested over the dorsum of the hind paw: the space between the first and second metatarsals (medial), the second and third metatarsals (central), and the fourth and fifth metatarsals (lateral). After a site was tested in one hind paw, the same site was immediately tested in the contralateral hind paw. The testing protocol was medial dorsum right then left, central dorsum right then left, lateral dorsum right then left, medial dorsum left then right, central dorsum left then right, and lateral dorsum left then right. The 6 measurements for each hind paw were averaged for the mean temperature. Hind paw temperature data were analyzed as the difference between the fractured side and the contralateral unfractured side.

2.8. Flow-cytometry analysis

After behavioral tests at 3 weeks post fracture, whole blood was collected with ethylenediaminetetraacetic acid (EDTA; 250 mM) into 1.5-mL tubes and transferred into 5-mL round-bottomed tubes. Whole blood was diluted 1:10 with red blood cell lysis buffer (Sigma-Aldrich, St. Louis, MO, USA), gently mixed for 1 minute, and then incubated for 10 minutes until translucent. The samples were diluted with Hanks balanced salt solution (HBSS; Gibco, Life Technologies, Grand Island, NY, USA) and centrifuged at 400*g* for 5 minutes. The supernatant was discarded and the pellet washed 3 times with fluorescence-activated cell sorting (FACS) buffer (5% fetal bovine serum and 0.02% sodium azide in phosphate-buffered saline [PBS]), then transferred into a fresh 5-mL round-bottomed FACS tube for staining. Splenocytes were collected from whole spleen and passed through a 50-μm filter with HBSS. Cells were pelleted by centrifugation at 400*g* for 5 minutes, resuspended in 1 mL red blood cell lysis buffer (Sigma-Aldrich), and incubated for 10 minutes. Cells were diluted in HBSS, washed 3 times with FACS buffer, and transferred to fresh 5-mL tubes for staining. Prepared samples were kept on ice and in the dark during the staining procedure. Briefly, about 1×10^6 cells were stained in 150 μL FACS buffer. Unconjugated CD16/CD32 (0.5 μL, FC block) was added and incubated for 15 minutes. Conjugated antibodies for staining were thoroughly mixed, then aliquoted to each sample (1 μL each

antibody/sample). Samples were incubated in the dark on ice for 30 minutes. One mL of FACS buffer was added per sample, then cells were pelleted by centrifugation at 400*g* for 5 minutes. The cells were washed 2 more times, and then analyzed on a BD Fortessa flow cytometer (BD Biosciences, San Jose, CA, USA).

Antibodies used for FACS were: Fc blocker, purified rat antimouse CD16/CD32 Clone 2.4G2, FITC rat anti-mouse CD3 (BD Biosciences), APC-cy7 rat anti-mouse CD4 (BD Biosciences), Pacific blue rat anti-mouse CD8, APC rat anti-mouse CD19 (eBioscience, San Diego, CA, USA), PE-cy7 Armenian hamster anti-human/rat/mouse CD27 (eBioscience), and APC rat anti-human/mouse CD45R (B220) (eBioscience).

2.9. Tissue processing and immunofluorescence confocal microscopy

To assess CD20+ B-cells infiltration and C5b-9 deposition in the sciatic nerve and hind paw skin at 3 weeks after fracture, mice were euthanized and immediately perfused with 4% paraformaldehyde (PFA) in PBS, pH 7.4, via the ascending aorta; the sciatic nerve, hind paw skin including sub-dermal layers was removed and post-fixed in 4% PFA for 2 hours, and then the tissues were treated with 30% sucrose in PBS at 4 °C before embedding in optimum cutting temperature (OCT) compound (Sakura Finetek, Torrance, CA, USA). Following embedding, 10-μm thick slices were made using a cryostat, mounted onto Superfrost microscope slides (Fisher Scientific, Pittsburgh, PA, USA), and stored at −80 °C. To examine if B cells were present in bone callus, tibial bones, including the fracture site, were excised with surrounding soft tissue, fixed with 4% PFA at 4 °C for 48 hours and decalcified in a 1:1 solution of 4% PFA and 14% EDTA at 4 °C for 3 weeks. After equilibration in 30% sucrose in PBS, bones were embedded in OCT compound, then cut into 12-μm sagittal slices, mounted onto Superfrost microscope slides, and stored at −80 °C. Spleen was collected and prepared as positive control for CD20 immunostaining.

Frozen sections were permeabilized and blocked with PBS containing 10% donkey serum and 0.3% Triton X-100 before primary antibody incubation. Sections were incubated either with polyclonal rabbit anti-CD20, 1:200 (Abcam, Cambridge, MA, USA) or polyclonal rabbit anti-C5b9, 1:250 (Abcam) diluted in PBS containing 2% serum at 4 °C overnight. After washing in PBS, the sections were incubated with donkey anti-rabbit immunoglobulin G conjugated with Dylight 547, 1:500 (Jackson ImmunoResearch Laboratories, West Grove, PA, USA) at room temperature and counterstained with DAPI (diluted 1:3000; Thermo Scientific, Waltham, MA, USA) to locate nuclei. After 3 washes, the sections were mounted with anti-fade mounting medium (Invitrogen, Life Technologies). Images were visualized and captured using a confocal microscope (Zeiss LSM710, Carl Zeiss, Jena, Germany). Control experiments included incubation of slices in primary and secondary antibody-free solutions, both of which led to low-intensity nonspecific staining patterns in preliminary experiments (data not shown).

2.10. Enzyme immunoassay

Mouse hind paw skin was collected and frozen immediately on dry ice. Skin tissue was cut into fine pieces in ice-cold PBS, pH 7.4, containing a cocktail of protease inhibitors (Roche Applied Science, Indianapolis, IN, USA) and followed by homogenization using a Polytron

device (Brinkmann Instruments, Westbury, NY, USA). Homogenates were centrifuged at 12,000*g* for 15 minutes at 4 °C and supernatant fractions were frozen at −80 °C until required for enzyme-linked immunosorbent assay (ELISA) performance. An aliquot was subjected to protein assay (Bio-Rad Laboratories Inc, Hercules, CA, USA) to normalize mediator levels. Interleukin (IL)-1β, IL-6, and tumor necrosis factor-α protein levels were determined using ELISA kits (R&D Systems, Minneapolis, MN, USA), C5b-9 membrane attack complex (MAC) levels were detected using C5b-9 ELISA kits (MyBioSource, San Diego, CA, USA), and the nerve growth factor (NGF) concentrations were measured by using the ChemiKine NGF ELISA kit (Millipore, Billerica, MA, USA) according to the manufacturer's instructions. The results of these assays were confirmed by repeating each experiment twice.

2.11. Western blot analysis

Mouse hind paw skin and sciatic nerve were harvested at 3 weeks after fracture (n = 4/group) and stored at −80 °C. All tissues were homogenized in ice-cold Tris buffer with 0.7% (v/v) β-mercaptoethanol and 10% glycerol. Lysates were centrifuged at 13,000*g* for 15 minutes at 4 °C, and the protein concentration of the supernatant was measured by a Bio-Rad DC protein assay reagent (Bio-Rad). Equal amounts of protein (50 μg) were size fractionated by sodium dodecyl sulfate-polyacrylamide gel electrophoresis and transferred onto a polyvinylidene difluoride membrane. The blots were blocked overnight with 5% normal serum in Tris-buffered saline with 0.5% Tween-20, and incubated with primary antibodies against immunoglobulin M (IgM) or β-actin (Santa Cruz Biotechnology, Dallas, TX, USA) for 1 hour on a rocking platform at room temperature. After 3 washes, the blots were incubated with secondary antibody for 1 hour at room temperature. The membrane was then washed again, and proteins were detected using ECL chemiluminescence reagent (GE Healthcare, Pittsburgh, PA, USA). The band intensities were quantified using ImageJ (National Institutes of Health, Bethesda, MD, USA).

2.12. Statistical analysis

For simple comparisons of 2 means, unpaired Student *t*-tests were performed. For more complex datasets we used 2-way analysis of variance or 2-way repeated-measures analysis of variance with Bonferroni corrections as detailed in the figure legends. All data are presented as the mean ± SEM, and differences are considered significant at a P value < 0.05 (Prism 6, GraphPad Software, La Jolla, CA, USA).

3. Results

3.1. Blood lymphocyte subsets are unchanged after fracture

First we determined whether peripheral lymphocyte subsets were altered in the fracture mice. Using flow cytometry, we analyzed lymphocyte subsets in the peripheral blood of control and 3-week postfracture mice. As shown in Fig. 1, the percentages of several circulating peripheral blood lymphocyte populations, including total T cells (Fig. 1A), T-helper cells (Fig. 1B), T-effector cells (Fig. 1C), B cells (Fig. 1D, F), and plasmablasts (Fig. 1E), were not different between 3-week postfracture mice and controls.

3.2. Anti-CD20 treatment depletes peripheral B cells

To evaluate the ability of anti-CD20 monoclonal antibody rituximab to deplete B cells in the mouse model of CRPS, we treated fracture/cast mice with one dose of anti-CD20 (200 μg/100 μL/ mouse) or control antibody at 1 week after fracture. Mice were sacrificed at 3 weeks after fracture to monitor the efficacy of antiCD20 mediated B-cell depletion in peripheral blood and spleen. As noted in Fig. 2A and C, flow cytometry analysis demonstrated that the abundance of CD20 B cells dramatically decreased to nearly undetectable levels in both blood and spleen 3 weeks after fracture (2 weeks after antibody injection). Quantification analysis (Fig. 2B, D) of flow cytometry B-cell data showed that anti-CD20 IgG treatment significantly depleted B cells in both blood ($P < 0.001$) and spleen ($P < 0.001$) in the fracture/cast mice.

3.3. Anti-CD20 prevents CRPS-like changes 3 weeks after fracture

Taking advantage of the anti-CD20 antibody, we examined the hypothesis that B cells are required for the development of CRPS-like changes in the mouse fracture/cast CRPS model. One dose of anti-CD20 or control IgG was administered systemically (tail vein injection) 1 week after fracture. Nociceptive and vascular changes were evaluated 3 weeks after fracture (1 day after cast removal). In preliminary experiments we did not observe any effects resulting from the injection of IgG alone on mechanical thresholds (−0.02 ± 0.07 in no fracture/no treatment, n = 8 vs 0.02 ± 0.09 in no fracture/IgG, n = 10), weight bearing (100.1 ± 0.35 in no fracture/no treatment, n = 8 vs 100.4 ± 0.25 in no fracture/IgG, n = 10), warmth (−0.02 ± 0.1 in no fracture/no treatment, n = 8 vs 0.05 ± 0.05 in no fracture/IgG, n = 10) or edema (0.01 ± 0.03 in no fracture/no treatment, n = 8, vs −0.004 ± 0.003 in no fracture/IgG, n = 10). As shown in Fig. 3, there were no lateralized nociceptive or vascular changes observed in the nonfracture animals treated with either control IgG or anti-CD20. After tibia fracture and 3 weeks cast immobilization, the control IgG-treated mice developed hind paw mechanical allodynia (Fig. 3A, $P < 0.001$), unweighting (Fig. 3B, $P < 0.001$), warmth (Fig. 3C, $P < 0.001$), and edema (Fig. 3D, $P < 0.001$). However, anti-CD20 B-cell depletion significantly reduced these nociceptive and vascular changes [significant main effect of treatment: $F(1, 47) = 292.05$, $P < 0.001$ for mechanical allodynia; $F(1, 47) = 166.28$, $P < 0.001$ for unweighting; $F(1, 46) = 8.65$, $P < 0.01$ for warmth; and $F(1, 48) = 71.42$, $P < 0.001$ for edema], suggesting a role for B cells in the development of postfracture CRPS-like changes.

3.4. Reduction of CRPS-like changes in B-cell-deficient μMT fracture mice

A complementary approach using transgenic B-cell deficient (μMT) mice was undertaken to further address the B-cell autoimmunity hypothesis. In this experiment, both μMT and wild-type mice were fractured and casted for 3 weeks, with wild-type and μMT nonfractured mice used as controls. Fig. 4 presents the effects of fracture and cast immobilization on nociceptive and vascular changes at 3 weeks post fracture in the μMT and wild-type mice. In the wild-type animals, tibia fracture caused chronic allodynia and hind paw unweighting (Fig. 4A, $P < 0.001$ and 4B, $P < 0.001$) and vascular changes (Fig. 4C, $P < 0.05$ and 4D, $P < 0.05$) in the injured limbs, whereas B-cell-deficient mice undergoing fracture had attenuated hind paw mechanical allodynia [significant main effect of strain: $F(1, 28) = 8.6$, $P < 0.01$;

Fig. 4A] and unweighting [significant main effect of strain: $F(1, 31) = 98.09$, $P < 0.001$; Fig. 4B], and no hind paw warmth developed: $F(1, 33) = 7.90$, $P < 0.01$; Fig. 4C.

3.5. Delayed anti-CD20 therapy reduces CRPS-like changes

Next, we investigated the therapeutic efficacy of anti-CD20 on established nociceptive and vascular changes in the CRPS model. Fracture mice were treated with a single dose of either anti-mouse CD20 or control IgG at 3 weeks post fracture, that is, 1 day after cast removal when maximal postfracture CRPS-like changes are established. Intact animals treated with control IgG or anti-CD20 served as controls. Hind paw nociceptive testing and assessment of warmth and edema were performed at baseline prior to fracture, again at 3 weeks post fracture the day after cast removal immediately prior to injection, and during the 28-day period following Ig injection. Fig. 5 demonstrates that a single intravenous anti-CD20 injection alleviated hind paw mechanical allodynia [significant main effect of treatment: $F(1, 100) = 39.7$, $P < 0.001$; Fig. 5A] and unweighting [significant main effect of treatment: $F(1, 101) = 42.50$, $P < 0.001$; Fig. 5B] between days 7 and 21 after treatment. Hind paw warmth [$F(1, 101) = 0.05$, $P = 0.83$; Fig. 5C] and edema [$F(1, 101) = 0.12$, $P = 0.73$; Fig. 5D] were not altered when B cells were depleted in this delayed fashion in fracture mice. There were no effects of control IgG or anti-CD20 over the time course of the experiment. This finding indicates that B cells are required not only for the development, but the maintenance of at least the nociceptive CRPS-like symptoms in the fracture CRPS model.

3.6. B-cell depletion does not alter postincision nociception

We next sought to determine if the antinociceptive effects of CD20+ cell depletion observed in the fracture/cast model were generalizable to a more acute model of pain after trauma. For this purpose we selected the hind paw incisional model of postsurgical pain [45]. CD20+ cells were depleted by injection of anti-CD20 or control antibody 24 hours prior to incision as described for the fracture/cast animals. Depletion of the CD20+ target cells occurs extremely rapidly after antibody administration and reaches a nadir by approximately 24 hours after injection [47]. Animals then underwent unilateral hind paw incision, and mechanical nociceptive withdrawal thresholds were followed until they approximated control levels. Hind paw incision induced a sustained mechanical allodynia that lasted for 6 days [significant main effect of surgery: $F(1, 10) = 131.89$, $P < 0.001$]. However, there were no differences seen between the control and CD20+ depleted incised groups [$F(1, 10) = 131.89$, $P = 0.35$; Fig. 6]. No effects of anti-CD20 were observed on the thresholds of the contralateral nonincised paws (data not shown).

3.7. B cells appear near the site of bone callus after fracture

We sought to determine if B cells infiltrated tissues ipsilateral to fracture and cast immobilization. For these experiments we targeted our detection efforts against the same CD20 antigen used to deplete B cells in the preceding studies. As a control experiment we stained splenic tissue. Inspection of the splenic sections revealed abundant CD20-positive cells, as expected (Fig. 7A). Positive staining was also found near the site of the healing fracture in the bone callus (Fig. 7B), and rare CD20+ cells were seen in sciatic nerves (Fig.

7C). There was no evidence of B-cell infiltration in the hind paw skin 3 weeks after fracture (Fig. 7D).

3.8. Immune complex deposition in the limbs of fracture mice

To determine if immune complexes indicative of autoimmunity could be found in skin and sciatic nerve tissue in the CRPS model, we analyzed IgM protein levels in these tissues from intact wild-type, fracture, and B-cell-deficient (μMT) fracture mice using Western blot analysis. As shown in Fig. 8, the basal levels of IgM were low in intact skin from control mice, whereas at 3 weeks post fracture, we observed remarkably increased IgM levels in the hind paw skin (Fig. 8A, $P < 0.001$) and sciatic nerve (Fig. 8B, $P < 0.001$) tissue ipsilateral to fracture. The levels of IgM were unaltered in tissues contralateral to fracture. In the μMT fracture mice, IgM content was not detected in tissues after fracture, confirming that B cells were the source of the IgM. Additional experiments failed to reveal evidence of IgG accumulation after fracture in wild-type mice (data not shown). Taken together with observations from behavioral studies, these data indicate that CD20-positive B cells produce IgM antibodies after fracture, which, in turn, ultimately support the CRPS-like changes in the murine fracture/cast model.

3.9. B-cell depletion does not alter inflammatory mediator levels

Previous studies in tibia fracture rodent models and CRPS patients showed upregulation of IL-1, IL-6, tumor necrosis factor-α, and NGF-β in the skin of involved limbs [35–38, 53, 54]. Given the observations of IgM deposition in skin tissue, we determined whether B cells contribute to the postfracture production of these inflammatory mediators. Groups of control and fracture mice were treated with either control IgG or anti-CD20 at 1 week post fracture. Hind paw skin ELISA assays on skin 3 weeks after fracture demonstrated significant elevations in IL-1β and NGF (both $P < 0.05$) in IgG-treated mice. As shown in Fig. 9, anti-CD20 did not block the enhanced production of these cytokines. Likewise, the administration of anti-CD20 had no effect on skin cytokine levels.

3.10. Complement membrane attack complex deposition in tissues from the limbs of fracture mice

Since our experiments examining the relationship between cytokines, NGF, and B-cell activity did not show a functional link to established CRPS-related mediators in skin, we probed an alternative mechanism. It has been shown that IgM is an effective activator of the complement system [56], and complement fragments such as C3a, C5a, and the membrane attack complex (C5b-9, MAC) support nociceptive sensitization in various systems [23, 58]. We hypothesized that complement system activation, using MAC formation as an index, might show enhanced activity in the CRPS model, and that B cells may support any observed activation. Using ELISA analysis, we demonstrated increased C5b-9 protein deposition in hind paw skin (Fig. 10A, $P < 0.05$) and sciatic nerve (Fig. 10C, $P < 0.01$) of the fracture mice. Anti-CD20 itself had no effect on C5b-9 levels in these tissues. However, anti-CD20 prevented the upregulation of C5b-9 in skin and sciatic nerve after fracture. Using immunohistochemistry and confocal microscopy, we detected increased C5b-9

protein deposition throughout the epidermis of the hind paw and sciatic nerve ipsilateral to fracture (Fig. 10B, D).

4. Discussion

Despite decades of study, CRPS remains a highly enigmatic syndrome. Its signs and symptoms are difficult to relate to any single molecule, tissue, or organ. Available treatments are poorly effective. Improving our understanding of the events supporting CRPS may help us to understand the perplexing nature of the condition's manifestations and suggest new avenues to treatment. In the present studies we provide evidence supporting the following conclusions: 1) B cells play a role in controlling the nociceptive and vascular CRPS-like changes occurring in the fracture and cast immobilization CRPS mouse model, but do not support these changes after simple soft tissue injury; 2) abundant B cells can be found near the site of the healing fracture and scattered in sciatic nerves, but there is little evidence of ongoing B-cell infiltration in other tissues; 3) the upregulation of inflammatory mediators in skin previously functionally implicated in CRPS is not reliant upon B-cell activity, suggesting additional mechanisms are at work; 4) IgM autoantibodies present in CRPS model mice may be directed against as-yet unidentified targets in the skin and sciatic nerves in the ipsilateral but not contralateral limbs; and 5) B cells support complement activation, to a degree, in the CRPS model. These findings are consistent with the hypothesis that B-cell-mediated autoantibody production supports the CRPS-like changes in a fracture-cast model of CRPS.

Many other medical conditions characterized by pain involve autoimmunity, and in that regard, the autoimmune hypothesis of CRPS is not without precedent. Rheumatoid arthritis is an example of a multisystem disease involving autoimmunity, in which pain is felt to be secondary to inflammation in joint tissues, though this relationship is complex [34]. Several autoimmune neuropathies and channelopathies provide examples of pain resulting more directly from autoimmune processes. For example, Guillain-Barré syndrome (GBS) is a polyneuropathy generally involving weakness, but sometimes, painful sensory symptoms and autonomic changes as well [24]. Autoantibodies have been identified in variable percentages of patients with GBS against neurofascin, gliomedin, contactin, GM1 ganglioside, and several additional proteins [10, 68]. Complement activation and subsequent cellular damage may then occur [25]. Interestingly, GBS is more frequent after certain viral and bacterial infections, for example, cytomegalovirus and *Campylobacter jejuni*, presumably due to the cross-reactivity of disease-fighting antibodies with neuronal cell proteins [5, 43]. Limited clinical evidence suggests a similar postinfectious (or postimmunization) preponderance of CRPS cases [12, 49, 57, 63]. In the case of paraneoplastic neuropathies, autoimmunity involving anti-Hu and anti-CV2/CRIMP5 antibodies have been linked to sensory changes involving pain [31]. Recently, a rare syndrome of idiopathic pain caused by a mix of anti-voltage-gated potassium channel complex antibodies was described [28]. Nearly 50% of patients with such antibodies had pain, and nearly 1/3 had pain as the only presenting symptom. However, neither this syndrome nor the other autoimmune neuropathies mentioned show the frequent relationship to trauma, the distinct regional manifestations, or the transition from an acute to a chronic phase characteristic of CRPS. Furthermore, not all peripheral nervous system autoimmunity

leads to dysfunction; naturally occurring antimyelin autoantibodies foster functional recovery after sciatic nerve trauma [66].

Our first step in detecting a possible autoimmune contribution to the CRPS-like features of the mouse fracture/cast model involved the depletion of CD20-expressing B cells. The human anti-CD20 medication rituximab potently reduces B-cell populations and, though not a first-line treatment, has been used successfully to treat autoimmune diseases such as rheumatoid arthritis and multiple sclerosis [21, 33]. We complemented experiments using anti-CD20 with the use of μMT mice, a strain of animals with a targeted mutation (*Ighm*^{tm1Cgn}) leading to mature B-cell deficiency and loss of IgM production. Both the use of anti-CD20 and the use of μMT mice show reductions in disease activity in other murine models of autoimmune disease such as rheumatoid arthritis [42, 60]. The 2 strategies showed significant and qualitatively similar efficacies in partially preventing nociceptive sensitization as well as the elevated temperature and edema in the affected paws of the CRPS model animals. Our results showing the slow reversal of nociceptive changes after anti-CD20 administration to mice with established CRPS-like changes are consistent with a slow depletion of circulating autoantibodies, as is seen in K/BxN spontaneously arthritic mice after anti-CD20 treatment [22]. Flow cytometry did not, however, demonstrate significant changes in a range of circulating T- and B-cell subsets in the CRPS model, which is similar to the picture in CRPS patients. Similarly, T-helper cells, T-effector cells, B cells, and natural killer cells were observed to be unchanged in CRPS patients in several studies [26, 48, 50]. However, an increase in a subset of monocytes (CD14+CD16+) and a decrease in the abundance of IL-2-producing T-helper cells were reported in CRPS patients [26, 50]. Our studies did not examine levels of other cell populations such as stem cells that might regulate the phenotypes under study.

We also analyzed skin and sciatic nerve samples both ipsi- and contralateral to the side of fracture for evidence of antibody deposition consistent with other autoimmune conditions. Our studies focused on IgM levels because several neuropathies are associated with IgM antibodies (eg, anti-myelin-associated glycoprotein, antisulfatide, anti-gangliosides) [39]. It should be noted that depletion of B cells with anti-CD20 does not selectively deplete IgM. We detected greatly increased quantities of IgM in both the skin and sciatic nerve tissues ipsilateral to the tibial fracture, but no increase on the contralateral side. Given that 1) maximal effects of CD20 depletion occur about 1 week after anti-CD20 injection in the CRPS model, 2) the half-life of IgM has been estimated to be between 2 and 8 days [2, 8, 67], and 3) the time to effect of exogenously administered autoantibodies in models of other painful conditions involving peripheral inflammation like arthritis is several days [41, 44], it is reasonable to postulate that the CD20-positive B cells do not directly modulate nociceptive sensitization, but ultimately support the CRPS-like changes in the murine fracture/cast model through the production of IgM antibodies. Presuming the involved antibodies to be distributed throughout the circulation, these observations may indicate that the levels of existing antigens in the affected limbs are strongly upregulated or that neoantigens are expressed in skin, sciatic nerve, and possibly other tissues after fracture and immobilization. We do not at this time know the identities of these antigens, however. It is notable that purified IgG from chronic CRPS patients enhances hyperalgesia and edema in

the injured limbs of mice when passively administered [61], although we did not identify an autoimmune contribution to sensitization after incision in our experiments. Moreover, our initial studies have focused on IgM because of the strong literature implicating this isotype in autoimmune disease. Moving forward, it will be necessary to compare the roles of both IgM and IgG in patients and rodent models of CRPS.

Because IgM is particularly effective at complement activation [69], and this activation in turn leads to the formation of complement fragments and C5b-9 membrane attack complexes on the surface of cellular membranes, causing subsequent cellular damage [13], we looked at changes in C5b-9 content in the hind paw skin and sciatic nerve after fracture and the role of B cells in mediating these changes. We observed a significant increase of C5b-9 protein deposition in the fracture side skin and sciatic nerve, and there was a moderate reduction of C5b-9 in skin (~25%) and slight reduction in sciatic nerve (~15%) caused by anti-CD20 treatment. Perhaps the moderate reduction in complement activation in skin is responsible for the partial reversal of nociceptive sensitization seen in B-cell-depleted mice. On the other hand, it is possible that complement activation is occurring after fracture in part via pathways other than the “classical” pathway, including the “alternative” and “lectin” pathways, thus not requiring the binding of autoantibodies to initiate the cascade. A related possibility is that autoantigen expression and autoantibody binding follow, rather than precede, complement system activation, as may be the case in synovial cells from patients with rheumatoid arthritis [51]. In contrast to the results for complement, we did not observe that skin cytokine levels either in control nonfracture or in CRPS model animals were altered by CD20 depletion. Additional pilot studies failed to show changes in anti-inflammatory cytokines such as IL-4 and IL-10.

A growing number of clinical reports suggest autoimmune contributions to CRPS. Autoantibodies can be found in the sera of some patients with CRPS; IVIG has shown promise as a treatment for this condition, and additional immunological changes in the blood and affected tissues suggest activation of the adaptive immune system [14, 15–17, 30]. The predilection of CRPS for females is also consistent with an autoimmune etiology. Beyond CRPS, a number of additional enigmatic pain syndromes may be supported by autoimmune mechanisms such as fibromyalgia and certain types of headaches [3, 6, 32]. By pursuing autoimmunity as a contributor to CRPS, we may uncover important new components of the disease process, delineate novel mechanisms for activation of the adaptive system of immunity, and discover new approaches to treatment of this disabling condition.

Acknowledgments

This study was supported by National Institutes of Health grants NS072168 and NS072143, and Department of Veterans Affairs, Rehabilitation Research, and Development Merit grant F7137R.

References

1. Bean DJ, Johnson MH, Kydd RR. The outcome of complex regional pain syndrome type 1: a systematic review. J Pain. 2014; 15:677–690. [PubMed: 24530407]
2. Brekke OH, Sandlie I. Therapeutic antibodies for human diseases at the dawn of the twenty-first century. Nat Rev Drug Discov. 2003; 2:52–62. [PubMed: 12509759]

3. Buskila D, Sarzi-Puttini P. Fibromyalgia and autoimmune diseases: the pain behind autoimmunity. Isr Med Assoc J. 2008; 10:77–78. [PubMed: 18300581]
4. Calder JS, Holten I, McAllister RM. Evidence for immune system involvement in reflex sympathetic dystrophy. J Hand Surg Br. 1998; 23:147–150. [PubMed: 9607647]
5. Caudie C, Quittard Pinon A, Taravel D, Sivadon-Tardy V, Orlikowski D, Rozenberg F, Sharshar T, Raphael JC, Gaillard JL. Preceding infections and anti-ganglioside antibody profiles assessed by a dot immunoassay in 306 French Guillain-Barre syndrome patients. J Neurol. 2011; 258:1958–1964. [PubMed: 21516465]
6. Chen WH, Chen YT, Lin CS, Li TH, Lee LH, Chen CJ. A high prevalence of autoimmune indices and disorders in primary nummular headache. J Neurol Sci. 2012; 320:127–130. [PubMed: 22841415]
7. Cossins L, Okell RW, Cameron H, Simpson B, Poole HM, Goebel A. Treatment of complex regional pain syndrome in adults: a systematic review of randomized controlled trials published from June 2000 to February 2012. Eur J Pain. 2013; 17:158–173. [PubMed: 23042687]
8. Curtis J, Bourne FJ. Half-lives of immunoglobulins IgG, IgA and IgM in the serum of new-born pigs. Immunology. 1973; 24:147–155. [PubMed: 4685369]
9. de Rooij AM, Florencia Gosso M, Haasnoot GW, Marinus J, Verduijn W, Claas FH, van den Maagdenberg AM, van Hilten JJ. HLA-B62 and HLA-DQ8 are associated with Complex Regional Pain Syndrome with fixed dystonia. PAIN®. 2009; 145:82–85. [PubMed: 19523767]
10. Devaux JJ, Odaka M, Yuki N. Nodal proteins are target antigens in Guillain- Barre syndrome. J Peripher Nerv Syst. 2012; 17:62–71. [PubMed: 22462667]
11. Dirckx M, Stronks DL, Groeneweg G, Huygen FJ. Effect of immunomodulating medications in complex regional pain syndrome: a systematic review. Clin J Pain. 2012; 28:355–363. [PubMed: 22001668]
12. Forster M, Umnus A, Siebrecht D, Baron R, Wasner G. A case of pain, motor impairment, and swelling of the arm after acute herpes zoster infection. PAIN®. 2012; 153:2478–2481. [PubMed: 22980745]
13. Fosbrink M, Niculescu F, Rus H. The role of c5b-9 terminal complement complex in activation of the cell cycle and transcription. Immunol Res. 2005; 31:37–46. [PubMed: 15591621]
14. Goebel A, Baranowski A, Maurer K, Ghiai A, McCabe C, Ambler G. Intravenous immunoglobulin treatment of the complex regional pain syndrome: a randomized trial. Ann Intern Med. 2010; 152:152–158. [PubMed: 20124231]
15. Goebel A, Blaes F. Complex regional pain syndrome, prototype of a novel kind of autoimmune disease. Autoimmun Rev. 2013; 12:682–686. [PubMed: 23219953]
16. Goebel A, Netal S, Schedel R, Sprotte G. Human pooled immunoglobulin in the treatment of chronic pain syndromes. Pain Med. 2002; 3:119–127. [PubMed: 15102158]
17. Goebel A, Stock M, Deacon R, Sprotte G, Vincent A. Intravenous immunoglobulin response and evidence for pathogenic antibodies in a case of complex regional pain syndrome 1. Ann Neurol. 2005; 57:463–464. [PubMed: 15732112]
18. Guo TZ, Offley SC, Boyd EA, Jacobs CR, Kingery WS. Substance P signaling contributes to the vascular and nociceptive abnormalities observed in a tibial fracture rat model of complex regional pain syndrome type I. PAIN®. 2004; 108:95–107. [PubMed: 15109512]
19. Guo TZ, Wei T, Kingery WS. Glucocorticoid inhibition of vascular abnormalities in a tibia fracture rat model of complex regional pain syndrome type I. PAIN®. 2006; 121:158–167. [PubMed: 16472917]
20. Guo TZ, Wei T, Shi X, Li WW, Hou S, Wang L, Tsujikawa K, Rice KC, Cheng K, Clark DJ, Kingery WS. Neuropeptide deficient mice have attenuated nociceptive, vascular, and inflammatory changes in a tibia fracture model of complex regional pain syndrome. Mol Pain. 2012; 8:85. [PubMed: 23191958]
21. Gurcan HM, Keskin DB, Stern JN, Nitzberg MA, Shekhani H, Ahmed AR. A review of the current use of rituximab in autoimmune diseases. Int Immunopharmacol. 2009; 9:10–25. [PubMed: 19000786]

22. Huang H, Benoist C, Mathis D. Rituximab specifically depletes short-lived autoreactive plasma cells in a mouse model of inflammatory arthritis. Proc Natl Acad Sci USA. 2010; 107:4658–4663. [PubMed: 20176942]
23. Jang JH, Clark JD, Li X, Yorek MS, Usachev YM, Brennan TJ. Nociceptive sensitization by complement C5a and C3a in mouse. PAIN®. 2010; 148:343–352. [PubMed: 20031321]
24. Joseph SA, Tsao CY. Guillain-Barre syndrome. Adolesc Med. 2002; 13:487–494. [PubMed: 12270796]
25. Kaida K. Guillain-Barre and Fisher syndromes: update on the pathophysiological role of antiganglioside antibodies. Rinsho Shinkeigaku. 2012; 52:914–916. [PubMed: 23196466]
26. Kaufmann I, Eisner C, Richter P, Huge V, Beyer A, Chouker A, Schelling G, Thiel M. Lymphocyte subsets and the role of TH1/TH2 balance in stressed chronic pain patients. Neuroimmunomodulation. 2007; 14:272–280. [PubMed: 18239379]
27. Kingery WS, Davies MF, Clark JD. A substance P receptor (NK1) antagonist can reverse vascular and nociceptive abnormalities in a rat model of complex regional pain syndrome type II. PAIN®. 2003; 104:75–84. [PubMed: 12855316]
28. Klein CJ, Lennon VA, Aston PA, McKeon A, Pittock SJ. Chronic pain as a manifestation of potassium channel-complex autoimmunity. Neurology. 2012; 79:1136–1144. [PubMed: 22895588]
29. Kohr D, Singh P, Tschernatsch M, Kaps M, Pouokam E, Diener M, Kummer W, Birklein F, Vincent A, Goebel A, Wallukat G, Blaes F. Autoimmunity against the beta2 adrenergic receptor and muscarinic-2 receptor in complex regional pain syndrome. PAIN®. 2011; 152:2690–2700. [PubMed: 21816540]
30. Kohr D, Tschernatsch M, Schmitz K, Singh P, Kaps M, Schafer KH, Diener M, Mathies J, Matz O, Kummer W, Maihofner C, Fritz T, Birklein F, Blaes F. Autoantibodies in complex regional pain syndrome bind to a differentiation- dependent neuronal surface autoantigen. PAIN®. 2009; 143:246–251. [PubMed: 19375222]
31. Koike H, Tanaka F, Sobue G. Paraneoplastic neuropathy: wide-ranging clinicopathological manifestations. Curr Opin Neurol. 2011; 24:504–510. [PubMed: 21799410]
32. Kurtuncu M, Kaya D, Zuliani L, Erdag E, Icoz S, Ugurel E, Cavus F, Aysit N, Birisik O, Vincent A, Eraksoy M, Vural B, Akman-Demir G, Tuzun E. CACNA1H antibodies associated with headache with neurological deficits and cerebrospinal fluid lymphocytosis (HaNDL). Cephalalgia. 2013; 33:123–129. [PubMed: 23111027]
33. Leandro MJ, de la Torre I. Translational mini-review series on B cell-directed therapies: the pathogenic role of B cells in autoantibody-associated autoimmune diseases—lessons from B cell-depletion therapy. Clin Exp Immunol. 2009; 157:191–197. [PubMed: 19604258]
34. Lee YC. Effect and treatment of chronic pain in inflammatory arthritis. Curr Rheumatol Rep. 2013; 15:300. [PubMed: 23292816]
35. Li W, Shi X, Wang L, Guo T, Wei T, Cheng K, Rice KC, Kingery WS, Clark JD. Epidermal adrenergic signaling contributes to inflammation and pain sensitization in a rat model of complex regional pain syndrome. PAIN®. 2013; 154:1224–1236. [PubMed: 23718987]
36. Li WW, Guo TZ, Li XQ, Kingery WS, Clark JD. Fracture induces keratinocyte activation, proliferation, and expression of pro-nociceptive inflammatory mediators. PAIN®. 2010; 151:843–852. [PubMed: 20934254]
37. Li WW, Guo TZ, Liang D, Shi X, Wei T, Kingery WS, Clark JD. The NALP1 inflammasome controls cytokine production and nociception in a rat fracture model of complex regional pain syndrome. PAIN®. 2009; 147:277–286. [PubMed: 19853379]
38. Li WW, Sabsovich I, Guo TZ, Zhao R, Kingery WS, Clark JD. The role of enhanced cutaneous IL-1beta signaling in a rat tibia fracture model of complex regional pain syndrome. PAIN®. 2009; 144:303–313. [PubMed: 19473768]
39. Mannoor K, Xu Y, Chen C. Natural autoantibodies and associated B cells in immunity and autoimmunity. Autoimmunity. 2013; 46:138–147. [PubMed: 23186367]
40. Marinus J, Moseley GL, Birklein F, Baron R, Maihofner C, Kingery WS, van Hilten JJ. Clinical features and pathophysiology of complex regional pain syndrome. Lancet Neurol. 2011; 10:637–648. [PubMed: 21683929]

41. Nandakumar KS, Andren M, Martinsson P, Bajtner E, Hellstrom S, Holmdahl R, Kleinau S. Induction of arthritis by single monoclonal IgG anti-collagen type II antibodies and enhancement of arthritis in mice lacking inhibitory FcgammaRIIB. Eur J Immunol. 2003; 33:2269–2277. [PubMed: 12884302]
42. O'Neill SK, Glant TT, Finnegan A. The role of B cells in animal models of rheumatoid arthritis. Front Biosci. 2007; 12:1722–1736. [PubMed: 17127417]
43. Orlikowski D, Porcher R, Sivadon-Tardy V, Quincampoix JC, Raphael JC, Durand MC, Sharshar T, Roussi J, Caudie C, Annane D, Rozenberg F, Leruez-Ville M, Gaillard JL, Gault E. Guillain-Barre syndrome following primary cytomegalovirus infection: a prospective cohort study. Clin Infect Dis. 2011; 52:837–844. [PubMed: 21427390]
44. Petkova SB, Konstantinov KN, Sproule TJ, Lyons BL, Awwami MA, Roopenian DC. Human antibodies induce arthritis in mice deficient in the low-affinity inhibitory IgG receptor Fc gamma RIIB. J Exp Med. 2006; 203:275–280. [PubMed: 16476768]
45. Pogatzki EM, Raja SN. A mouse model of incisional pain. Anesthesiology. 2003; 99:1023–1027. [PubMed: 14508341]
46. Poree LR, Guo TZ, Kingery WS, Maze M. The analgesic potency of dexmedetomidine is enhanced after nerve injury: a possible role for peripheral alpha2-adrenoceptors. Anesth Analg. 1998; 87:941–948. [PubMed: 9768799]
47. Reff ME, Carner K, Chambers KS, Chinn PC, Leonard JE, Raab R, Newman RA, Hanna N, Anderson DR. Depletion of B cells in vivo by a chimeric mouse human monoclonal antibody to CD20. Blood. 1994; 83:435–445. [PubMed: 7506951]
48. Ribbers GM, Oosterhuis WP, van Limbeek J, De metz M. Reflex sympathetic dystrophy: is the immune system involved? Arch Phys Med Rehabil. 1998; 79:1549–1552. [PubMed: 9862298]
49. Richards S, Chalkiadis G, Lakshman R, Buttery JP, Crawford NW. Complex regional pain syndrome following immunisation. Arch Dis Child. 2012; 97:913–915. [PubMed: 22858647]
50. Ritz BW, Alexander GM, Nogusa S, Perreault MJ, Peterlin BL, Grothusen JR, Schwartzman RJ. Elevated blood levels of inflammatory monocytes (CD14+ CD16+) in patients with complex regional pain syndrome. Clin Exp Immunol. 2011; 164:108–117. [PubMed: 21303362]
51. Romero V, Fert-Bober J, Nigrovic PA, Darrah E, Haque UJ, Lee DM, van Eyk J, Rosen A, Andrade F. Immune-mediated pore-forming pathways induce cellular hypercitrullination and generate citrullinated autoantigens in rheumatoid arthritis. Sci Transl Med. 2013; 5:209ra150.
52. Sabsovich I, Clark JD, Liao G, Peltz G, Lindsey DP, Jacobs CR, Yao W, Guo TZ, Kingery WS. Bone microstructure and its associated genetic variability in 12 inbred mouse strains: microCT study and in silico genome scan. Bone. 2008; 42:439–451. [PubMed: 17967568]
53. Sabsovich I, Guo TZ, Wei T, Zhao R, Li X, Clark DJ, Geis C, Sommer C, Kingery WS. TNF signaling contributes to the development of nociceptive sensitization in a tibia fracture model of complex regional pain syndrome type I. PAIN®. 2008; 137:507–519. [PubMed: 18035493]
54. Sabsovich I, Wei T, Guo TZ, Zhao R, Shi X, Li X, Yeomans DC, Klyukinov M, Kingery WS, Clark JD. Effect of anti-NGF antibodies in a rat tibia fracture model of complex regional pain syndrome type I. PAIN®. 2008; 138:47–60. [PubMed: 18083307]
55. Schwartzman RJ, Erwin KL, Alexander GM. The natural history of complex regional pain syndrome. Clin J Pain. 2009; 25:273–280. [PubMed: 19590474]
56. Shulman MJ, Pennell N, Collins C, Hozumi N. Activation of complement by immunoglobulin-M is impaired by the substitution serine-406—asparagine in the immunoglobulin-mu heavy chain. Proc Natl Acad Sci USA. 1986; 83:7678–7682. [PubMed: 3094013]
57. Sibanc B, Lesnicar G. Complex regional pain syndrome and lyme borreliosis: two different diseases? Infection. 2002; 30:396–399. [PubMed: 12478332]
58. Sorkin LS, Otto M, Baldwin WM 3rd, Vail E, Gillies SD, Handgretinger R, Barfield RC, Ming Yu H, Yu AL. Anti-GD(2) with an FC point mutation reduces complement fixation and decreases antibody-induced allodynia. PAIN®. 2010; 149:135–142. [PubMed: 20171010]
59. Subbarao J, Stillwell GK. Reflex sympathetic dystrophy syndrome of the upper extremity: analysis of total outcome of management of 125 cases. Arch Phys Med Rehabil. 1981; 62:549–554. [PubMed: 6172092]

60. Svensson L, Jirholt J, Holmdahl R, Jansson L. B cell-deficient mice do not develop type II collagen-induced arthritis (CIA). Clin Exp Immunol. 1998; 111:521–526. [PubMed: 9528892]
61. Tekus V, Hajna Z, Borbely E, Markovics A, Bagoly T, Szolcsanyi J, Thompson V, Kemeny A, Helyes Z, Goebel A. A CRPS-IgG-transfer-trauma model reproducing inflammatory and positive sensory signs associated with complex regional pain syndrome. PAIN®. 2014; 155:299–308. [PubMed: 24145209]
62. van de Beek WJ, Roep BO, van der Slik AR, Giphart MJ, van Hilten BJ. Susceptibility loci for complex regional pain syndrome. PAIN®. 2003; 103:93–97. [PubMed: 12749963]
63. van de Vusse AC, Goossens VJ, Kemler MA, Weber WE. Screening of patients with complex regional pain syndrome for antecedent infections. Clin J Pain. 2001; 17:110–114. [PubMed: 11444711]
64. van Rooijen DE, Roelen DL, Verduijn W, Haasnoot GW, Huygen FJ, Perez RS, Claas FH, Marinus J, van Hilten JJ, van den Maagdenberg AM. Genetic HLA associations in complex regional pain syndrome with and without dystonia. J Pain. 2012; 13:784–789. [PubMed: 22795247]
65. Vaneker M, Wilder-Smith OH, Schrombges P, Oerlemans HM. Impairments as measured by ISS do not greatly change between one and eight years after CRPS-1 diagnosis. Eur J Pain. 2006; 10:639–644. [PubMed: 16300975]
66. Vargas ME, Watanabe J, Singh SJ, Robinson WH, Barres BA. Endogenous antibodies promote rapid myelin clearance and effective axon regeneration after nerve injury. Proc Natl Acad Sci USA. 2010; 107:11993–11998. [PubMed: 20547838]
67. Vieira P, Rajewsky K. The half-lives of serum immunoglobulins in adult mice. Eur J Immunol. 1988; 18:313–316. [PubMed: 3350037]
68. Yuki N. Guillain-Barre syndrome and anti-ganglioside antibodies: a clinician- scientist's journey. Proc Jpn Acad Ser B Phys Biol Sci. 2012; 88:299–326.
69. Zwart B, Ciurana C, Rensink I, Manoe R, Hack CE, Aarden LA. Complement activation by apoptotic cells occurs predominantly via IgM and is limited to late apoptotic (secondary necrotic) cells. Autoimmunity. 2004; 37:95–102. [PubMed: 15293879]

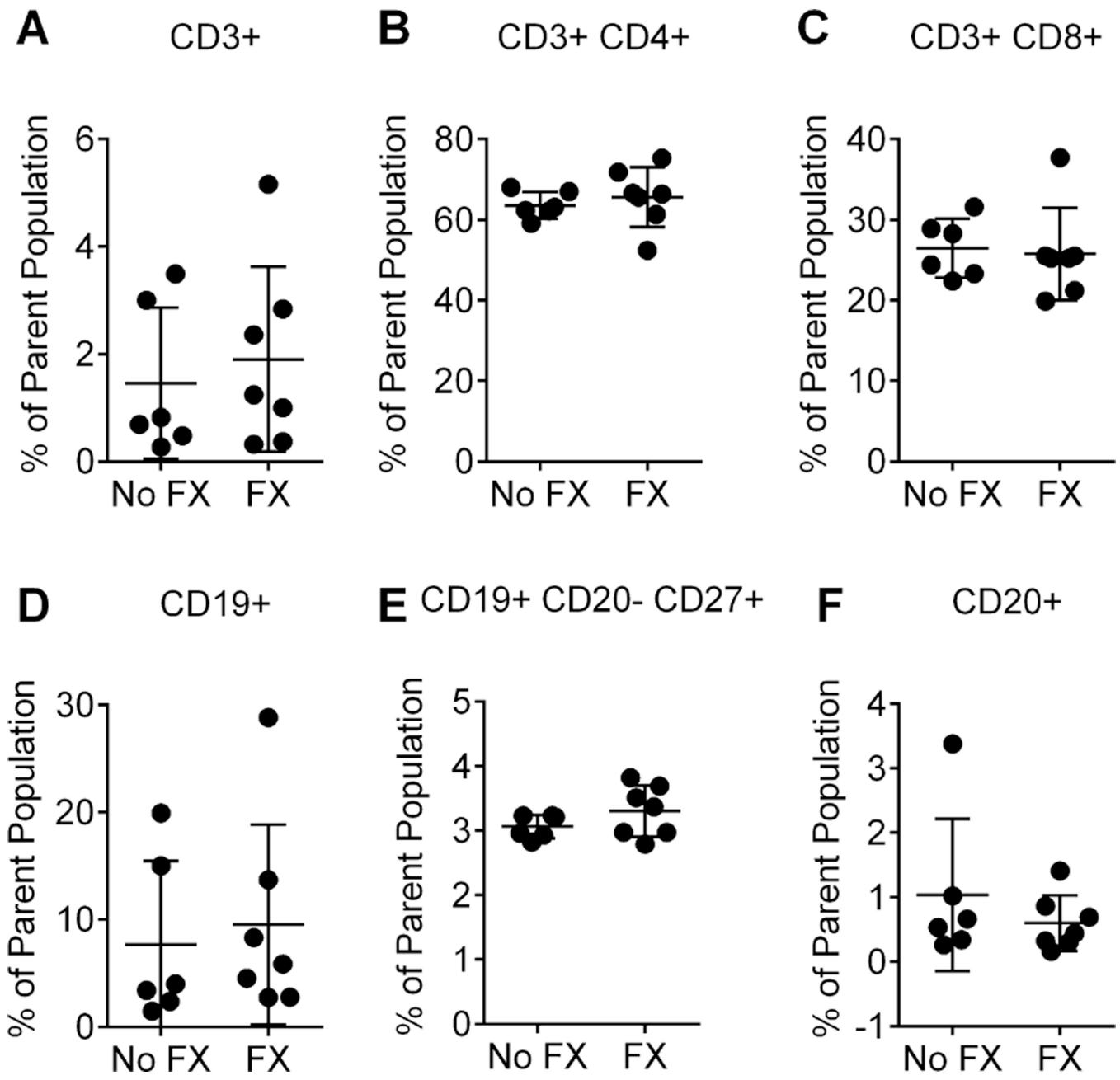

Fig. 1.

Flow cytometric analysis of peripheral blood lymphocyte populations in mice from controls (No FX) and 3 weeks post fracture (FX). Cells were stained with a combination of conjugated monoclonal antibodies, and analyzed by flow cytometry to identify various lymphocyte populations. (A) CD3+/total T cells as percentage of total lymphocytes; (B) CD3+CD4+/T helper cells; (C) CD3+CD8+/T effector cells; (D) CD19+/B cells as percentage of total lymphocytes; (E) CD19+CD20-CD27+/plasmablasts; (F) CD20+/ B cells as percentage of total lymphocytes. Compared with no-fracture control animals (n = 6), fracture did not induce changes in blood lymphocyte subsets (unpaired *t*-test, n = 7); error bars indicate SEM.

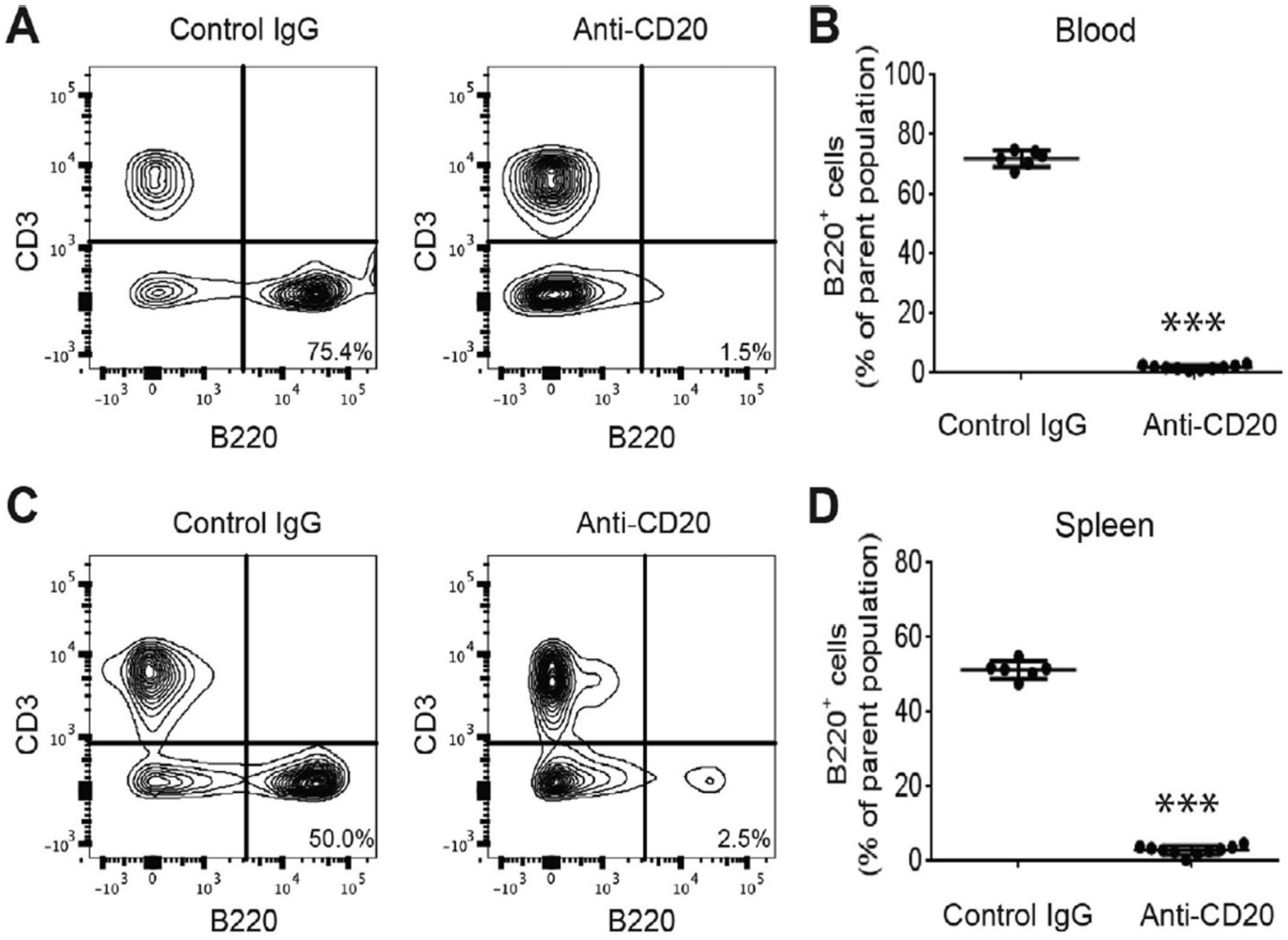

Fig. 2.

B-cell depletion in blood and spleen after CD20 antibody treatment in the complex regional pain syndrome mice. One group of fracture mice was treated with control antibody, another fracture group was treated with anti-CD20 antibody to deplete B cells at 1 week (after fracture) and flow cytometry performed 3 weeks after fracture. Shown in (A) and (C) are representative flow cytometry panels from blood and spleen, respectively, depicting the CD3+ T-cell population and the B220+ B-cell population of both groups. Treatment with CD20 antibody results in a strong reduction in B-cell numbers, as seen in the second panel. Quantification in (B) shows a significant decrease in the number of B220+ cells in the blood of FX-anti-CD20 mice (n = 10) compared to FX-IgG (n = 6) animals. Similarly, in (D), numbers of B220+ cells are strongly decreased in the spleen of FX-anti-CD20 mice (n = 10) compared to FX-IgG (n = 6) animals. Un-paired *t*-test, $^{***}P < 0.001$ for FX+antiCD20 vs FX+IgG. FX, fracture; IgG, immunoglobulin.

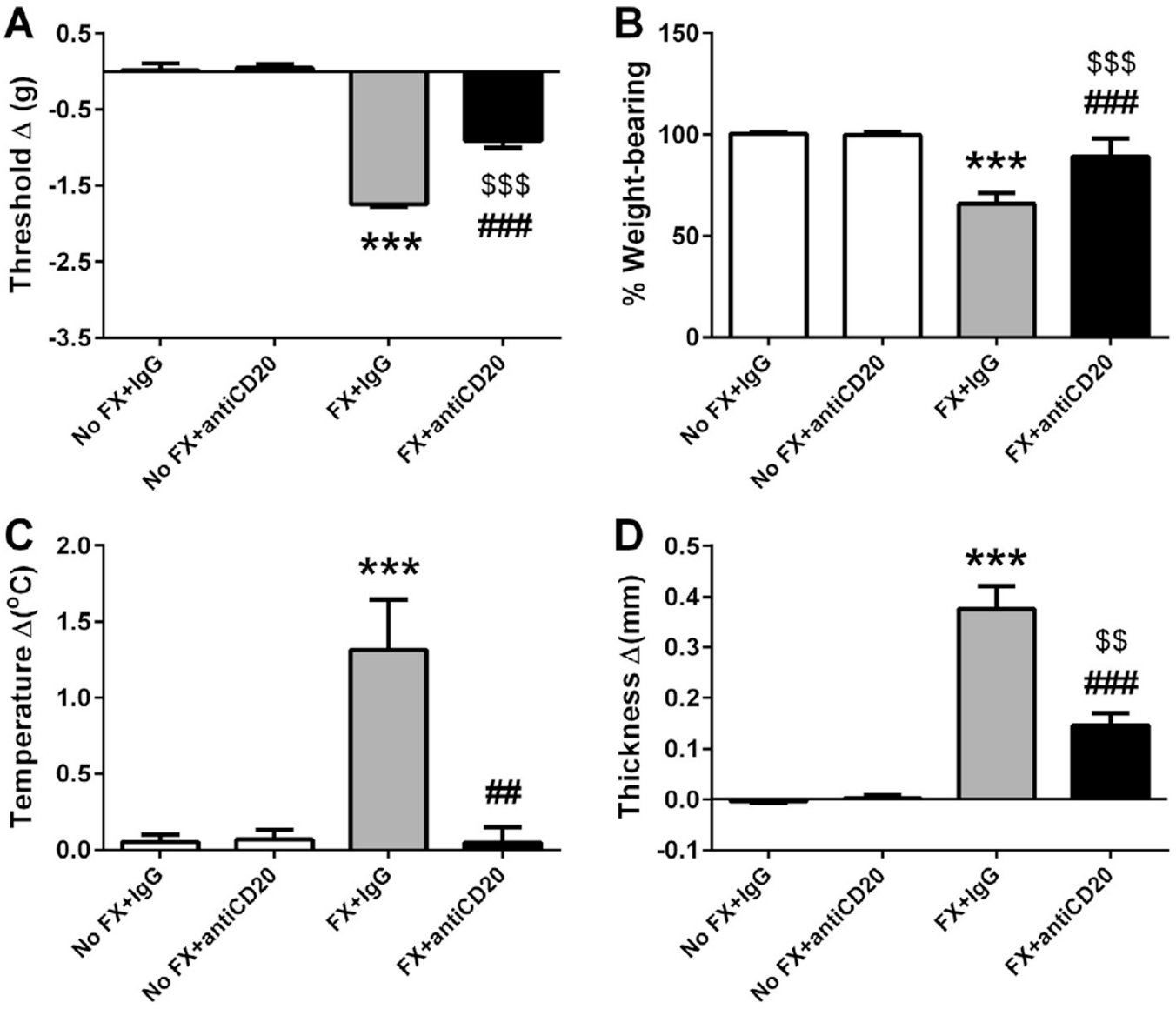

Fig. 3.

B-cell depletion with anti-CD20 partially blocked the nociceptive and vascular changes 3 weeks after fracture and cast immobilization. Mice underwent a right distal tibia fracture (FX) and were casted for 3 weeks. After 1 week of cast immobilization, fracture mice and intact controls (No FX) were treated with anti-mouse CD20 antibody or control immunoglobulin G (IgG; 200 μg/100 μL) via intravenous tail vein injection. Hind paw nociceptive testing and assessment of warmth and edema were performed at 3 weeks after fracture upon cast removal and on wild-type nonfractured mice. There were no nociceptive or vascular changes observed in the No FX control animals treated with control IgG or anti-CD20. After tibia fracture and 3 weeks cast immobilization, the control antibody-treated mice (n = 14) developed hind paw mechanical allodynia (A), unweighting (B), warmth (C), and edema (D). However, intravenous injection of anti-CD20 significantly reduced postfracture hind paw (n = 18) von Frey mechanical allodynia (A), unweighting (B), warmth (C), and edema (D). Measurements for (A), (C), and (D) represent the difference between

the fracture side and contralateral paws, thus, a positive value represents an increase in temperature or thickness on the fracture side; a negative value represents a decrease in mechanical nociceptive thresholds on the affected side. Measurements for (B) represent weight-bearing on the fracture hind limb as a ratio to 50% of bilateral hind limb loading, thus, a percentage lower than 100% represents hind paw unweighting. Data were analyzed using a 2-way analysis of variance with Bonferroni correction for post hoc contrasts. $^{***}P < 0.001$ for FX+IgG (n = 13–14) vs No FX+IgG (n = 10), $^{\$\$}P < 0.01$ and $^{\$\$\$}P < 0.001$ for FX +antiCD20 (n = 17–18) vs No FX+antiCD20 (n = 8–10), $^{\#\#}P < 0.01$ and $^{\#\#\#}P < 0.001$ for FX+antiCD20 (n = 17–18) vs FX+IgG (n = 13–14). Data are expressed as mean values ± SEM.

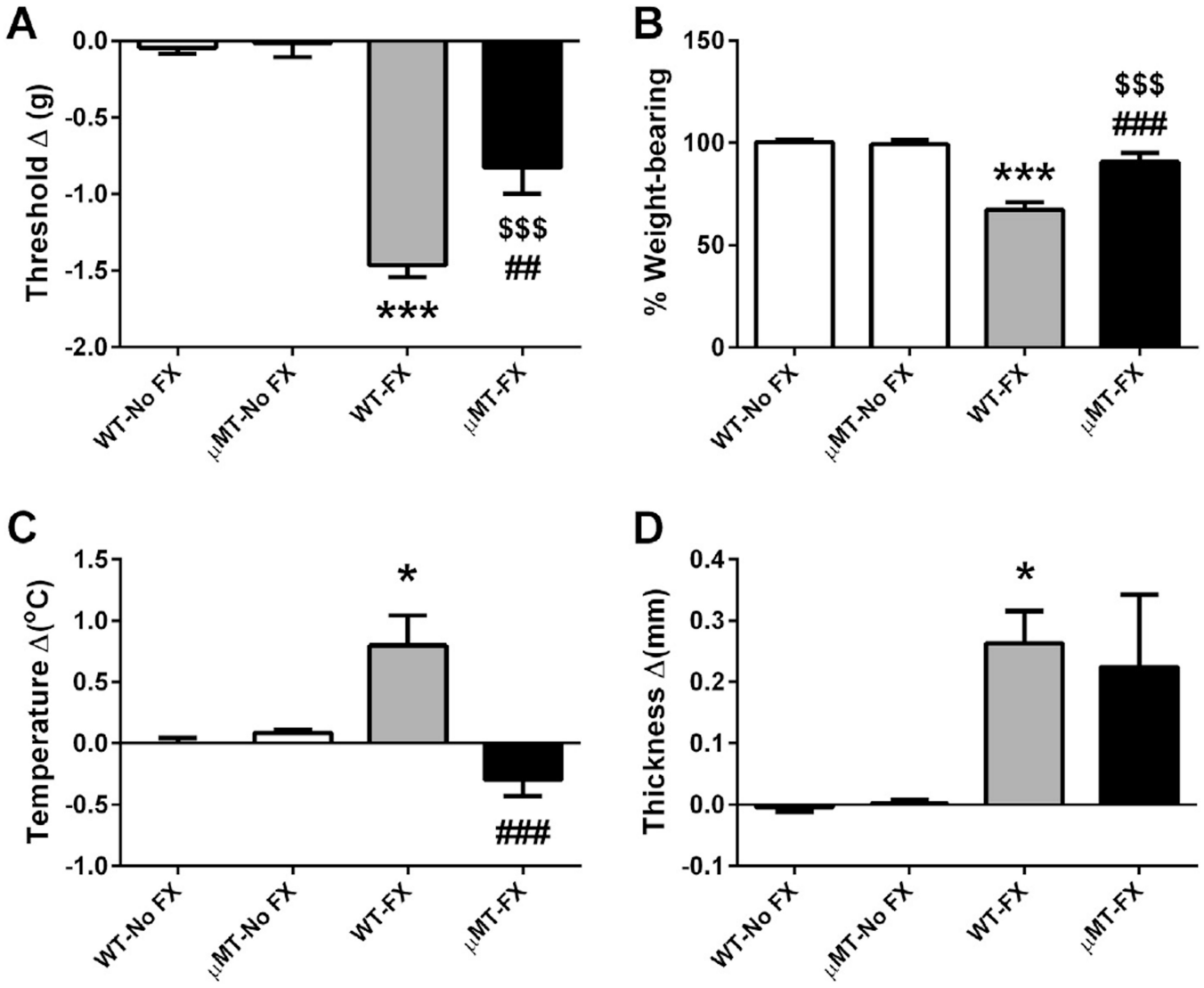

Fig. 4.

Nociceptive and vascular changes in B-cell-deficient μMT mice at 3 weeks after fracture. Wild-type (WT), and B-cell-deficient μMT mice underwent distal tibia fracture (FX) with hind limb casting for 3 weeks, then the cast was removed and behavioral testing performed; intact wild-type and μMT mice without fracture and cast immobilization served as controls. The methods for calculating the graphed values are described in Fig. 3. A 2-way analysis of variance was used to test the effects of fracture and B-cell-deficient transgenic mice on the dependent variables, with a Bonferroni correction for post hoc contrasts. There were no nociceptive or vascular changes observed in μMT-No FX mice compared to the WT-No FX controls. WT fracture (WT-FX) mice developed mechanical allodynia (A), unweighting (B), warmth (C), and edema (D), and B-cell-deficient μMT fracture (μMT-FX) mice exhibited a reduction in von Frey mechanical allodynia (A), unweighting (B), and warmth (C), but no changes on edema (D). $^{*}P < 0.05$ and $^{***}P < 0.001$ for WT-FX (n = 9–12) vs WT-No FX (n = 9), $^{\$\$\$}P < 0.001$ for μMT-FX (n = 9–12) vs μMT-No FX (n = 6), $^{\#\#}P < 0.01$ and $^{\#\#\#}P <$

0.001 for μMT-FX (n = 9–12) vs WT-FX (n = 9–11). Data are expressed as mean values ± SEM.

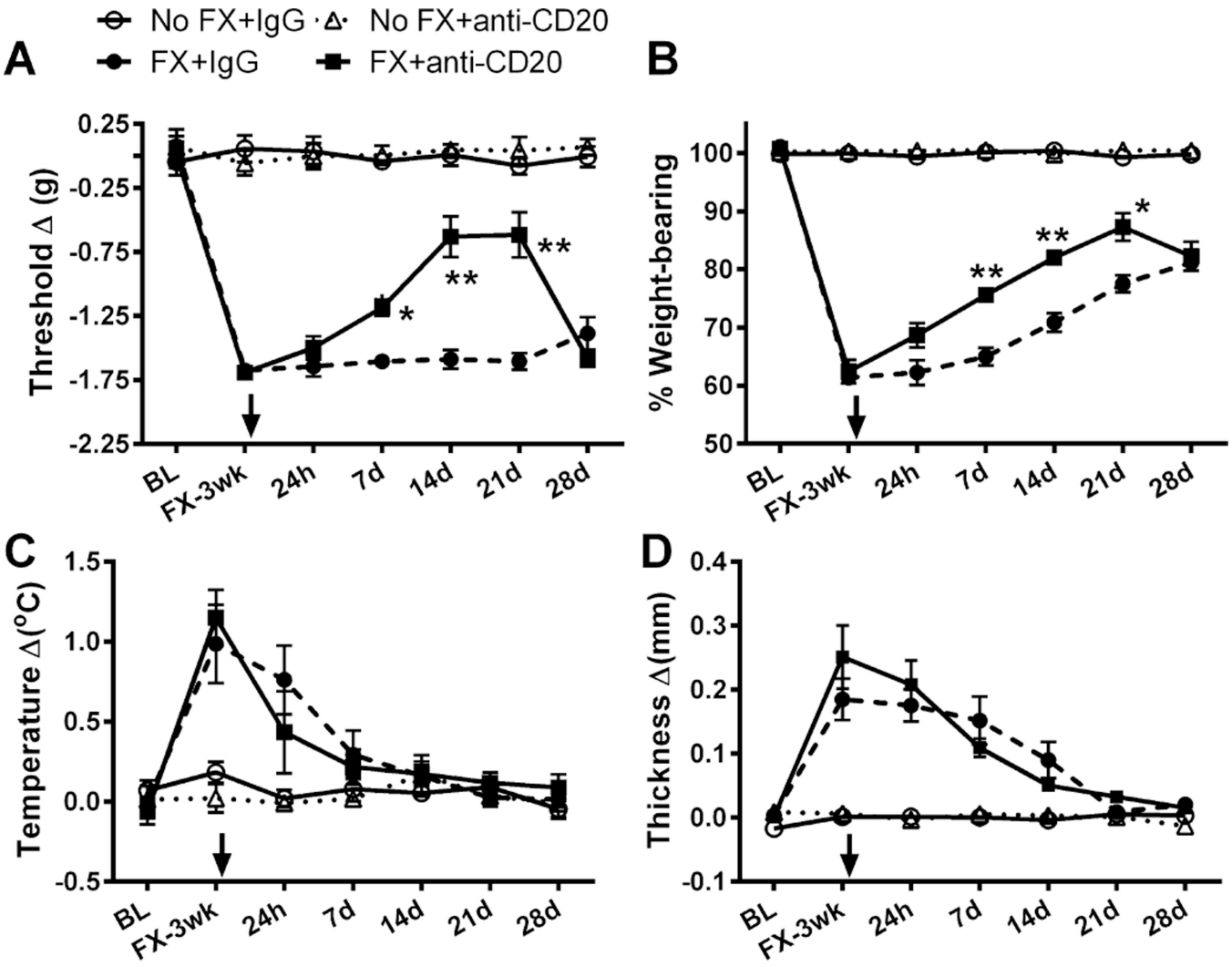

Fig. 5.

Prolonged effects of a single injection of anti-CD20 B-cell depletion therapy on nociceptive and vascular changes in the mouse model of complex regional pain syndrome. Mice underwent tibia fracture (FX) and were casted for 3 weeks; then the cast was removed. The next day they were treated with either an anti-mouse CD20 antibody, or a control immunoglobulin (IgG) at a dose of 200 μg/100 μL (intravenously), intact controls (No FX) treated with control IgG or anti-CD20 served as controls. Hind paw nociceptive testing and assessment of warmth and edema were performed prior to fracture, 3 weeks after fracture upon cast removal, and 24 hours and 7, 14, 21, and 28 days after intravenous anti-CD20 injection. The methods for calculating the graphed values are described in Fig. 3. A 2-way repeated-measures analysis of variance with post hoc Bonferroni correction demonstrated there were no effects of control IgG or anti-CD20 over the time course of the experiment in the non-FX mice, whereas significant ipsilateral hind paw allodynia (A), unweighting (B), warmth (C), and edema (D) were observed 3 weeks post fracture. Postfracture hind paw mechanical allodynia (A) and unweighting (B) were attenuated between 7 and 21 days after drug administration, but warmth (C) and edema (D) were not altered when B cells were

depleted in fracture mice. $^{*}P < 0.05$, $^{**}P < 0.01$, for FX+anti-CD20 (n = 8–10) vs FX+IgG (n = 8–10) at different time points after drug administration, respectively. Data are expressed as mean values ± SEM, and arrows indicate the time point where IgG or anti-CD20 was injected.

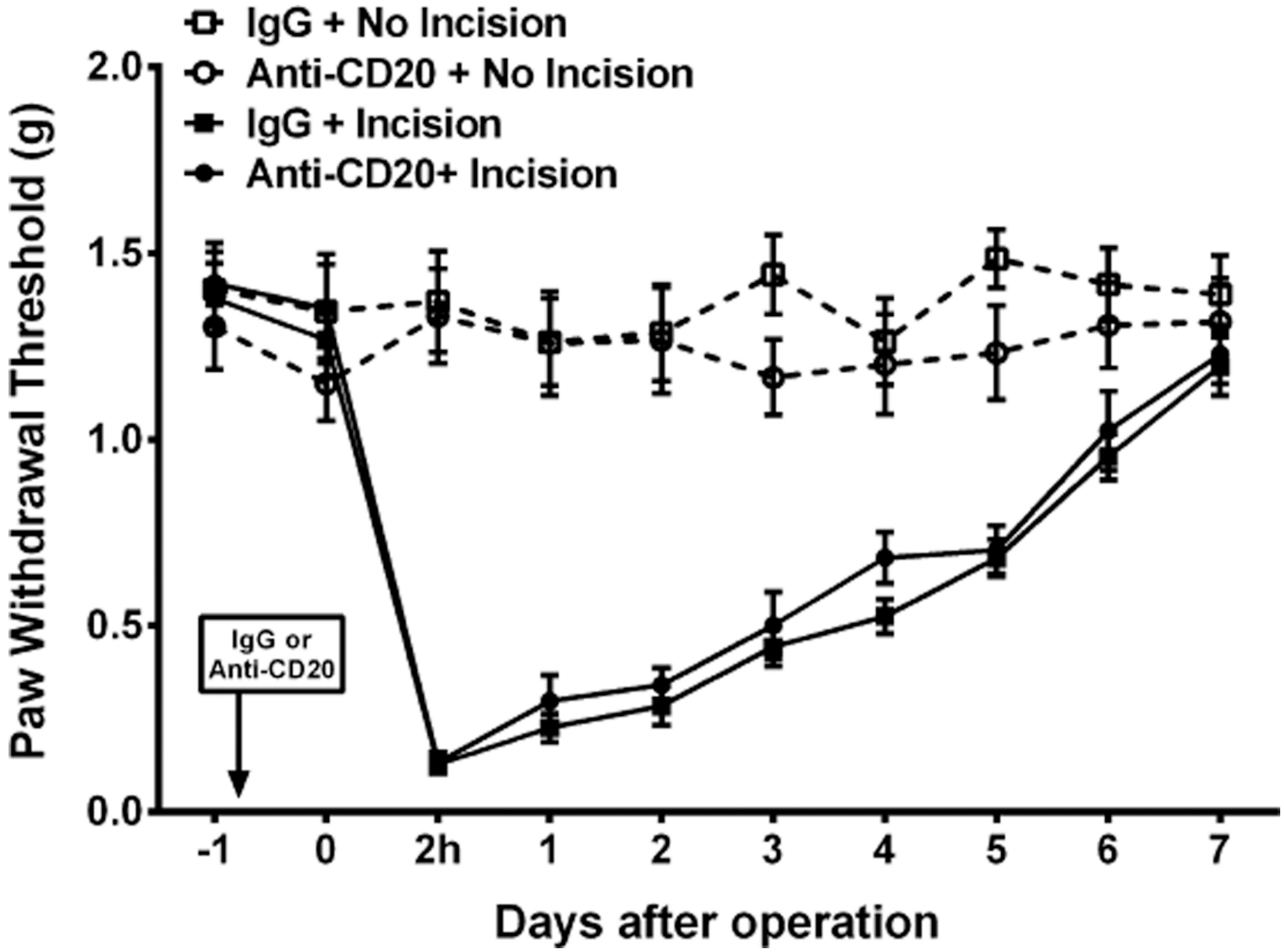

Fig. 6.

Anti-CD20 antibody treatment does not alter postincisional nociceptive sensitization. Mice received anti-CD20 (200 μg/100 μL) or vehicle (100 μL) once via tail vein injection 24 hours before performing the surgery/sham procedure. The hind paw incision model of postoperative pain was employed. Sham-treated mice were exposed to the same duration and concentration of anesthesia without performing incision. Mechanical sensitivity testing was performed daily (n = 6 per cohort). A 2-way repeated-measures analysis of variance with post hoc Bonferroni correction demonstrated significant ipsilateral hind paw allodynia after incision in both the immunoglobulin G (IgG) and the anti-CD20 antibody-injected mice. Data are expressed as mean values ± SEM.

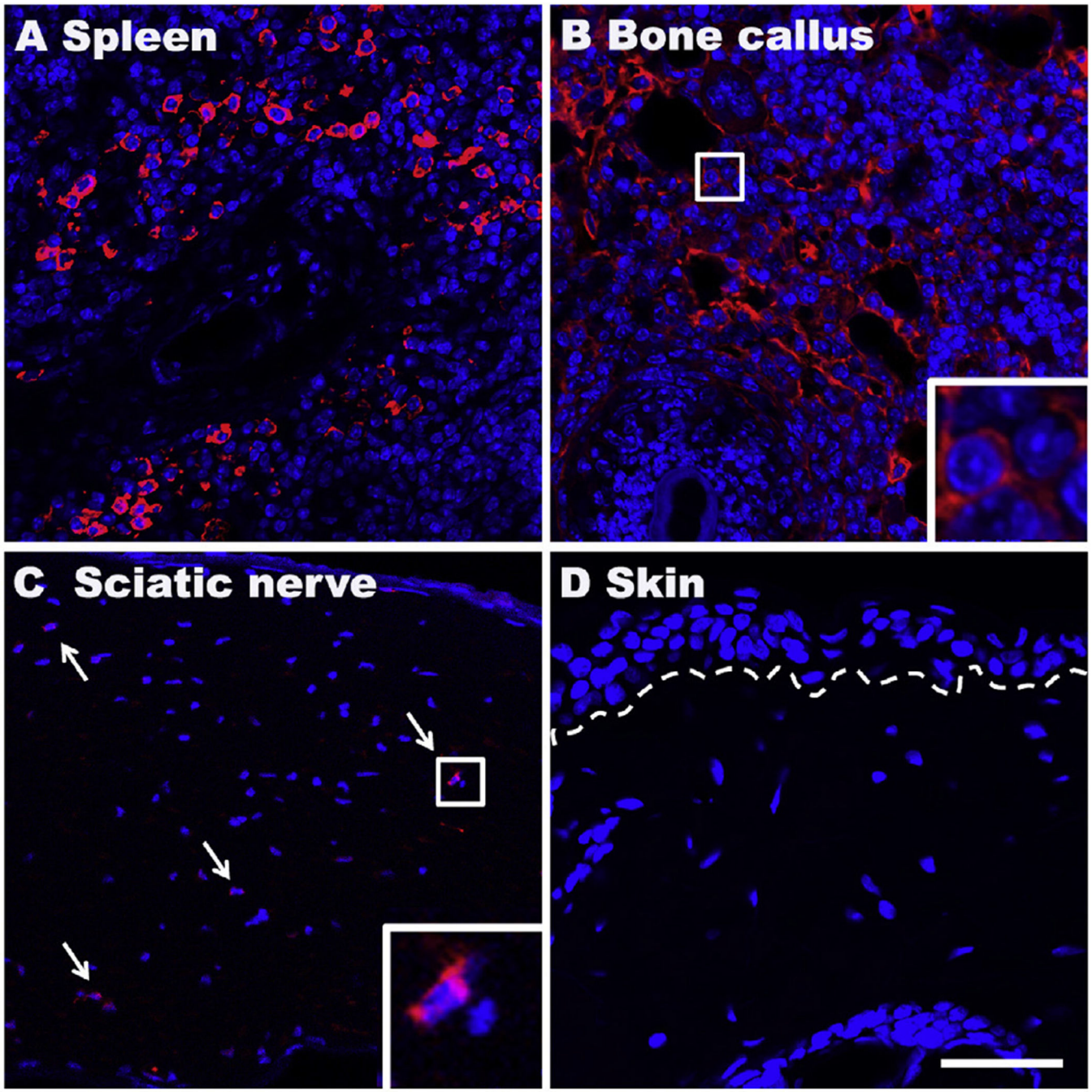

Fig. 7.

Representative fluorescent photomicrographs of immunostaining for the B-cell marker CD20 (red) at 3 weeks postfracture. DAPI (blue) counterstain was performed to show DNA content and nuclei. Abundant CD20 (cytoplasmic/red) positive B cells were observed in spleen (A) and bone callus near the site of fracture (B), and scattered B cells in sciatic nerves (C), but not seen in skin (D). Dotted line indicates the epidermal-dermal boundary, arrows: B cells, small boxed regions in panels (B) and (C) are shown enlarged in the lower right corner of the panels, respectively; scale bar = 50 μm.

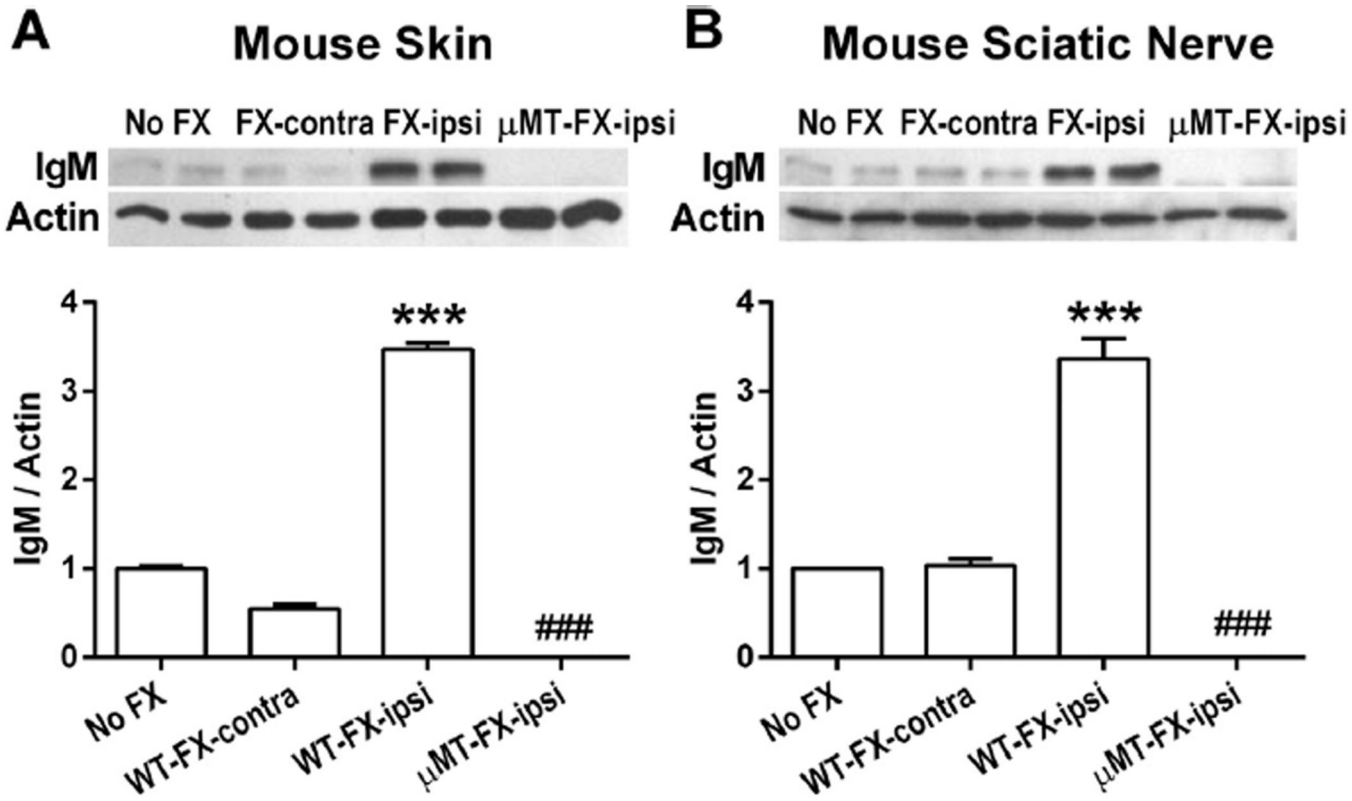

Fig. 8.

Western blot analysis of immunoglobulin M (IgM) protein levels in hind paw skin, and sciatic nerve at 3 weeks after fracture (FX). Compared with control wild-type mice (No FX), IgM protein levels were greatly increased in skin (A), and sciatic nerve (B) in wild-type mice ipsilateral to the fracture, but unchanged on the contralateral side. IgM bands were absent from skin (A), and sciatic nerve (B) tissue extracts from B-cell-deficient μMT mice after fracture. Data were analyzed using a 2-way analysis of variance with Bonferroni correction for post hoc contrasts. $^{***}P < 0.001$, for WT-FX-Ipsi (n = 4) vs No FX (n = 4), $^{###}P < 0.001$ for FX/μMT-ipsi (n = 4) vs WT-FX-Ipsi (n = 4). WT, wild type; Ipsi, ipsilateral to fracture; Contra, contralateral to fracture. Data are expressed as mean values ± SEM.

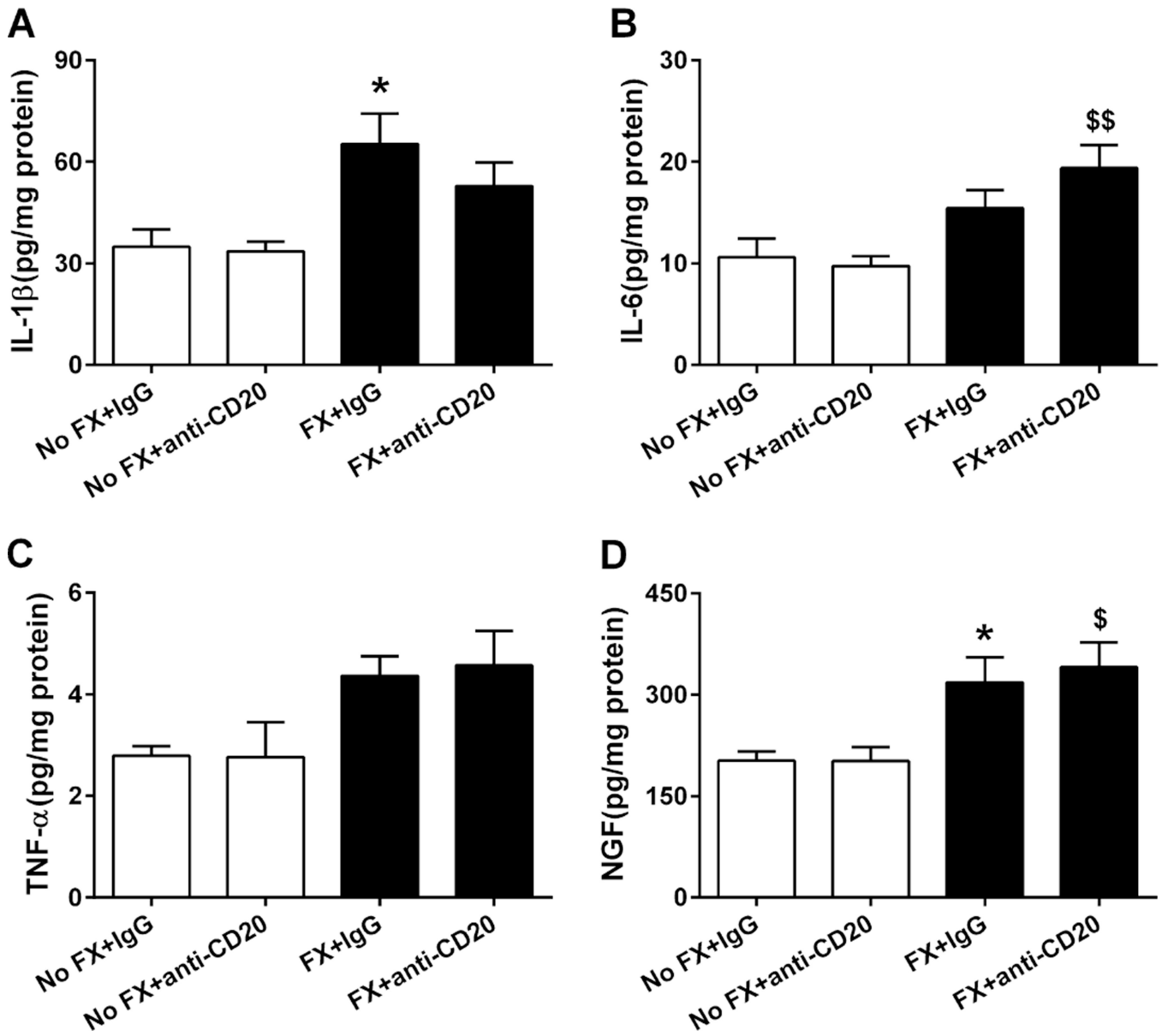

Fig. 9.

Enzyme-linked immunosorbent assay analysis for skin inflammatory cytokines and nerve growth factor (NGF) levels in fracture (FX) and control mice treated with either anti-CD20 or control immunoglobulin G (IgG; n = 8 per cohort). Anti-CD20 alone did not change cytokine levels in the controls. At 3 weeks post fracture, hind paw skin interleukin (IL)-1β (A), IL-6 (B), tumor necrosis factor (TNF)-α (C), and NGF (D) protein levels all were increased in fracture mice treated with control IgG, and anti-CD20 treatment had no effect on fracture induced upregulation of the cutaneous inflammatory mediators. Data were analyzed using a 2-way analysis of variance with Bonferroni correction for post hoc contrasts. $^{*}P < 0.05$ for FX+IgG (n = 8) vs No FX+IgG (n = 8), $^{\$}P < 0.05$, $^{\$\$}P < 0.01$, for FX+anti-CD20 (n = 8) vs No FX+anti-CD20 (n = 8). Data are expressed as mean values ± SEM.

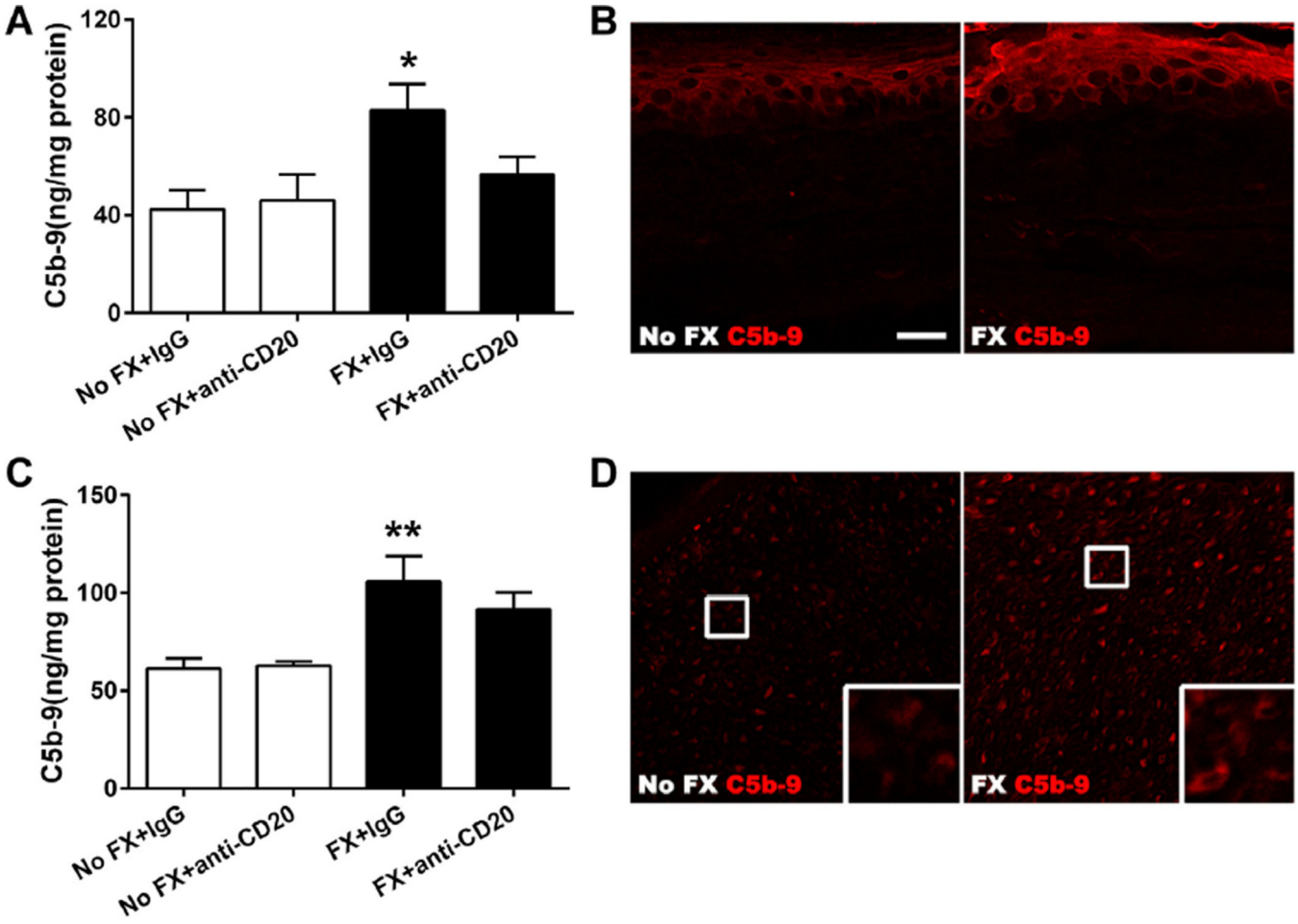

Fig. 10.

Changes in hind paw skin and sciatic nerve C5b-9 membrane attack complex protein levels in control (No FX) and fracture (FX) mice treated with either anti-CD20 or control immunoglobulin G (IgG). Panels (A) and (C): Anti-CD20 alone had no effects on C5b protein deposition in hind paw skin and sciatic nerve (n = 8 per cohort). At 3 weeks post fracture, skin and sciatic nerve C5b-9 protein levels were increased in mice treated with control IgG. Treatment with anti-CD20 prevented the induction of C5b in skin, but did not significantly change the induction of C5b-9 in sciatic nerve. Data were analyzed using a 2-way analysis of variance with Bonferroni correction test for post hoc contrasts; error bars indicate SEM. $^{*}P < 0.05$, and $^{**}P < 0.01$ for FX+IgG (n = 7) vs No FX+IgG (n = 7). Panels (B) and (D): Representative fluorescent photomicrographs of immunostaining for the C5b-9 (red) in hind paw skin and sciatic nerve at 3 weeks postfracture. No staining is shown with the secondary antibody alone (omitting the C5b-9 antibody, data not shown). There is an increase in C5b-9 protein deposition throughout the hind paw epidermis (B) and sciatic nerve (D) ipsilateral to fracture. Scale bar = 20 μm in both panels (B) and (D).